

LadderMIL: Multiple Instance Learning with Coarse-to-Fine Self-Distillation

Shuyang Wu¹, Yifu Qiu², Ines P. Nearchou³, Sandrine Prost¹

Jonathan A Fallowfield¹, David Harrison⁴, Hakan Bilen², Timothy J Kendall¹

¹Institute for Regeneration and Repair, University of Edinburgh, Edinburgh, UK

²School of Informatics, University of Edinburgh, Edinburgh, UK

³Indica Labs, 8700 Education Pl NW, Bldg. B Albuquerque, US

⁴Medical School, University of St Andrews, St Andrews, UK

¹{frank.wu, s.prost, jonathan.fallowfield, tim.kendall}@ed.ac.uk

²{yifu.qiu, h.bilen}@ed.ac.uk

³inearchou.wu@indicalab.com, ⁴david.harrison@st-andrews.ac.uk

Abstract

Multiple Instance Learning (MIL) for whole slide image (WSI) analysis in computational pathology often neglects instance-level learning as supervision is typically provided only at the bag level. In this work, we present **LadderMIL**, a framework designed to improve MIL through two perspectives: (1) *employing instance-level supervision* and (2) *learning inter-instance contextual information at bag level*. Firstly, we propose a novel **Coarse-to-Fine Self-Distillation (CFSD)** paradigm that probes and distills a network trained with bag-level information to adaptively obtain instance-level labels which could effectively provide the instance-level supervision for the same network in a self-improving way. Secondly, to capture inter-instance contextual information in WSI, we propose a **Contextual Encoding Generator (CEG)**, which encodes the contextual appearance of instances within a bag. We also theoretically and empirically prove the instance-level learnability of CFSD. Our LadderMIL is evaluated on multiple clinically relevant benchmarking tasks including breast cancer receptor status classification, multi-class subtype classification, tumour classification, and prognosis prediction. Average improvements of 8.1%, 11% and 2.4% in AUC, F1-score, and C-index, respectively, are demonstrated across the five benchmarks, compared to the best baseline. Code will be available after review.

1 Introduction

Computational pathology (CPATH) for the automated analysis of digital gigapixel whole slide images (WSIs) has demonstrated immense potential for precision medicine in fields typified by oncology [1, 2, 3, 4, 5]. In contrast to regular daily images, WSIs pose two challenges [6]. Firstly, as expert annotation of features within an image is costly, WSIs are typically annotated with slide-level labels. Secondly, due to their extremely high resolution, it is a common requirement to divide WSIs into multiple patches and compute an embedding for each patch independently through a feature encoder before concatenating these embeddings into frozen bag-level features (Figure 1a). Hence, the analysis of WSIs usually omits the online feature encoder and patches in negatively labelled bags are assumed to all be negative while at least one is assumed to be positive in positive bags. Multiple

instance learning (MIL) [7] has been the standard machinery to model WSIs as a bag of patches (or instances) and to learn classification of them from only bag-level supervision.

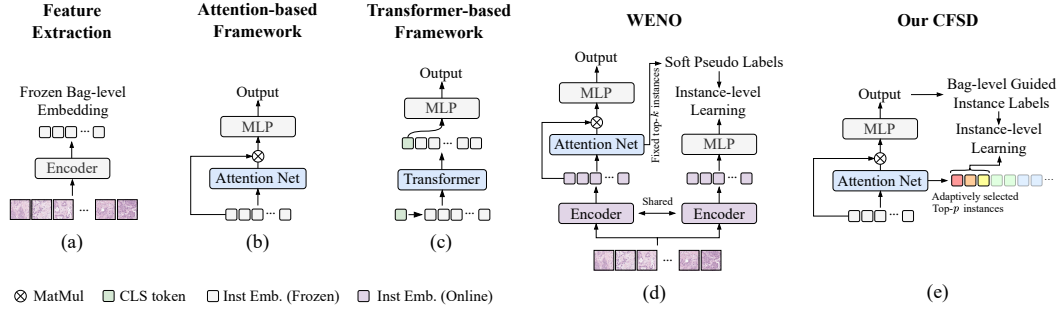


Figure 1: **Comparison of popular frameworks with our novel CFSD.** CFSD can efficiently introduce instance-level learnability by using self-distillation that takes one attention network to simultaneously learn knowledge from both bag-level and instance-level.

Most conventional MIL frameworks in CPATH are built on the success of deep networks. Due to the varying instance number, a pooling operation is commonly used in MIL to pool bag-level embeddings into a vector with fixed dimension. While maxpooling and average pooling are the most basic operations, the more successful techniques compute a weighted average of them by obtaining soft scores through various attention mechanisms. As shown in Figure 1, we compared our new method with three popular frameworks. The attention-based framework uses gated attention mechanisms [8, 9, 10, 11, 12], where the latent feature for classification is computed through matrix multiplying a bag-level attention map on bag-level features. Unlike these prior frameworks that independently process patches, vision transformers [13] have recently been applied to CPATH problems to capture correlations across instances through multi-head attention [14, 15]. However, these prior approaches suffer from poor instance classification as learning to classify at bag level does not guarantee accurate learning at instance level due to the attention pooling operation that incorporates the hypothesis space for bag-level features into the instance predictions [16].

A promising strategy to provide instance-level supervision is knowledge distillation [17], which uses information from a teacher network (the bag classifier) to assist the training of a student network (the instance classifier). Self-distillation is a further simplified technique based on knowledge distillation that allows simultaneous knowledge sharing between the teacher and student networks. WENO [18] follows the knowledge distillation strategy to train bag and instance classifiers, using the bag-level soft pseudo labels to guide the instance-level training. However, although WENO trains the feature encoder from scratch with shared parameters between the two branches, it differs from the routine workflow that a pre-trained backbone is applied to reduce computational costs [19, 20, 21, 22, 23]. Meanwhile, the selection of high-attention instances or instance-level learning is inflexible and manually determined using grid search.

In this paper, to flexibly enable instance-level supervision for MIL, we introduce a novel Coarse-to-Fine Self-Distillation (CFSD) framework which facilitates learning from coarser (bag-level) knowledge to finer (instance-level) knowledge in a self-improving manner. In the bag-level branch, CFSD actively probes and distills the attention network trained with bag-level information to obtain instance-level labels for high-confidence instances. In the instance-level branch, the same attention network serves as an instance-level classifier and the selected high-confidence instances are used for further instance-level training. Unlike WENO, we show that powerful performance can be achieved by applying self-distillation directly on an attention network shared by the bag-level and instance-level branches, even when using frozen features that better align with the current application context. Additionally, an adaptive threshold scheduling (ATS) mechanism is designed to automatically update the threshold for high-attention instance selection during training, from the initial top-5% to a maximum of top-20% depending on whether the model continues to improve, offering more flexibility than a grid search approach.

Furthermore, we leverage the advantages of transformer-based frameworks that use self-attention [24] and positional encoding to capture inter-instance contextual information at the bag level. With the idea of conditional positional encoding [25], PEG [25] and PPEG [14] gather information from neighbouring instances through reshaping feature sequences into square feature maps and applying

convolutional operations. However, we argue that given WSIs vary in aspect ratio and many instances not adjacent in their original two-dimensional position are regarded as neighbours after background removal in preprocessing, the result of convolution is inaccurate. To address this, we propose the Contextual Encoding Generator (CEG) using intra-bag normalised x and y coordinates to provide accurate positional information incorporating with the attention map obtained from CFSD to more precisely encode the contextual arrangement of instances within a bag.

With the integration of these modules, we propose LadderMIL, a hybrid framework capable of bag-level and instance-level learning in a self-improving way, with CFSD and CEG plugged in. We demonstrate the efficacy of LadderMIL using five benchmarking tasks, including an internal benchmark for breast cancer estrogen and progesterone receptor status classification, multi-class subtype classification (TCGA-RCC), tumour classification (CAMELYON16), and prognosis prediction (TCGA-LUAD). Our novel LadderMIL achieves the best performance across all benchmarks. Moreover, the instance-level learnability of LadderMIL is theoretically proven following Jang and Kwon [16], and empirically validated using the synthetic MNIST dataset.

Our main contributions are: (1) We propose CFSD and prove instance-level learnability both theoretically and empirically as a universal module that fits across various MIL frameworks. (2) We leverage the transformer-based framework, proposing CEG for the encoding of inter-instance contextual information. (3) We show that LadderMIL, which integrates both CFSD and CEG, achieves state-of-the-art performance on multiple benchmarking tasks, introducing average improvements of 8.1%, 11% and 2.4% in AUC, F1-score, and C-index, respectively.

2 Related Work

2.1 Instance-level Learnability in MIL

Recent studies have shown that the instance-level learnability of attention-based and transformer-based MIL models is not guaranteed, both theoretically and empirically [16]. This limitation arises from the attention pooling operation which multiplies attention weights over instance features, incorporating the hypothesis space for bag-level features into the instance predictions. While much effort has focused on improving MIL from the instance-level perspective, most work aims to fine-tune feature extractors to obtain better representations [26, 27, 28]. However, the MIL framework itself often remains based on conventional designs. These approaches are computationally expensive, which contradicts the goal of using MIL to reduce computational costs, especially with the availability of foundation models pre-trained on histopathological data [29, 30, 31, 32, 33]. Therefore, an efficient approach to enable instance-level learning is needed to enhance MIL’s overall capability, with self-distillation being a possible option.

DTFD-MIL [34] employs feature distillation for two-tier bag-level training, creating smaller pseudo-bags to alleviate the effects of limited cohort sizes. However, the training of DTFD-MIL still focuses only on bag level. In contrast, WENO [18] uses knowledge distillation between the bag and instance levels, which takes the attention scores from positive instances at bag-level classification to be the soft pseudo labels that guide instance-level training. However, in WENO, the acquisition of positive instances relies on grid searching for the optimal threshold, which is inflexible since the positive instance ratio across different datasets usually varies. Furthermore, the parameter share in WENO is performed on the feature encoder and trained from scratch, whereas the previously mentioned pre-trained foundation models are being more widely used for feature extraction, omitting the update of feature encoder [20, 21, 22, 23, 35]. In contrast to these existing methods, our CFSD is designed to train bag-level and instance-level classification on frozen features with a shared attention network, which uses self-distillation to improve the classifier instead of the feature encoder, and progressively introduces instance-level training by adaptively updating the threshold for high-attention instances selection, from top-5% to top-20%.

2.2 Positional Encoding in MIL

TransMIL [14] performs MIL using two transformer layers with Nyström-Attention [36] and a Pyramid Position Encoding Generator (PPEG) to encode positional information. The idea of positional encoding for images originated in the Vision Transformer (ViT), which splits images into square patches and preserves all background patches as valid [13]. In standard images where all parts of the

image are useful, this leads to only minor discontinuity between patches, except at row boundaries at the edge of the image. In contrast, when processing WSIs, non-informative and often abundant background patches without tissue are typically removed, creating significant discontinuities between the remaining patches containing informative tissue (see Figure 4), introducing noises into positional encoding. Although PPEG resizes bag-level features into two dimensions and processes them with convolutions, the positional encoding is still one-dimensional and treats the embeddings as a continuous sequence. This disregards the spatial discontinuities, preventing PPEG from effectively representing the two-dimensional feature map and leading to inaccuracies in convolution operations. Alternatively, our CEG utilises normalised two-dimensional coordinates with the bag-level attention map obtained from CFSD to better capture the inter-instance relationships at the bag level.

3 Methodology

3.1 Multiple-instance Learning (MIL)

Problem formulation. Taking binary classification as an example, given a bag of K instances that $X = \{x_1, x_2, \dots, x_K\}$, we would like to train a classifier that accurately predicts a bag-level target value $Y \in \{0, 1\}$ without access to instance-level labels $\{y_1, y_2, \dots, y_K\}$, where $y_k \in \{0, 1\}$, $k = 1, 2, \dots, K$. The MIL problem is defined as:

$$Y = \begin{cases} 0, & \text{iff } \sum_k y_k = 0, \\ 1, & \text{otherwise.} \end{cases} \quad (1)$$

Attention-based MIL. In computational pathology, a feature extractor with output dimension $1 \times D$ is used to create bag-level features $H = \{h_1, h_2, \dots, h_K\} \in \mathbb{R}^{K \times D}$, where h_k are instance-level embeddings. A fully connected layer is used as the first layer, reducing the embedding dimension to 512, such that $\mathbf{h} \in \mathbb{R}^{K \times 512}$. To implement MIL with attention [?], the attention network f_{attn} comprises three linear layers with parameters $\mathbf{U} \in \mathbb{R}^{256 \times 512}$, $\mathbf{V} \in \mathbb{R}^{256 \times 512}$ and $\mathbf{w} \in \mathbb{R}^{256 \times 1}$. The attention map $A_k \in \mathbb{R}^{K \times 1}$ and the attention-applied bag-level feature $\mathbf{M} \in \mathbb{R}^{1 \times 512}$ are expressed as:

$$A_k = f_{attn}(\mathbf{h}) = \frac{\exp\{\mathbf{w}^\top (\tanh(\mathbf{V}\mathbf{h}_k^\top) \odot \text{sigm}(\mathbf{U}\mathbf{h}_k^\top))\}}{\sum_{j=1}^K \exp\{\mathbf{w}^\top (\tanh(\mathbf{V}\mathbf{h}_j^\top) \odot \text{sigm}(\mathbf{U}\mathbf{h}_j^\top))\}} \quad (2)$$

$$\mathbf{M} = \sum_{k=1}^K A_k \mathbf{h}_k \quad (3)$$

Transformer-based MIL. The transformer-based MIL framework differs from attention-based designs. Following the framework of TransMIL [14] that composes transformer layer f_{NA} with Nyström-Attention(LN(\cdot)) and encodes position with PPEG, we construct our model using transformer layer f_{SA} composed as Self-Attention(LN(\cdot)) and using the contextual encoding generator (CEG) for inter-instance contextual information encoding. Let f_{cls} be the bag-level classifier, the classification made with TransMIL and our modified version are written as:

$$\hat{Y}_{\text{TransMIL}} = f_{cls}(f_{NA}(\text{PPEG}(f_{NA}(\cdot)))) \quad (4)$$

$$\hat{Y}_{\text{Ours}} = f_{cls}(f_{SA}(\text{CEG}(f_{SA}(\cdot)))) \quad (5)$$

3.2 Instance-level Learnable MIL

The attention-based framework has been widely used in previous work and it has been demonstrated that the attention network can highlight important instances related to the bag-level label [4, 9, 19, 37], suggesting it is reasonable to annotate high-attention instances with bag-level labels and use self-distillation for instance-level supervision in MIL. We also carried out a preliminary experiment to verify the principle in Appendix B.

Coarse-to-Fine Self-Distillation (CFSD). Building on the previous work, we introduce the novel CFSD approach to improve instance-level learnability in MIL. Based on the finding that the top- p instances are highly relevant to the prediction label Y , we apply an adaptive threshold scheduling

(ATS) method which updates p dynamically during training to select the top- p instances $H'_p \in \mathbb{R}^{P \times D}$ and their corresponding instance-level label $Y'_p \in \{0, 1\}$ from the bag H using the trained attention map A and bag-level label Y , where $p \in [5\%, 20\%]$. Initially, we set $p = 5\%$ (top-5%) to prioritise high-confidence instances, and the threshold p is incremented by 1% if the bag-level metrics no longer increase for three consecutive epochs, to a maximum of $p = 20\%$ (top-20%). In this way, we ensure instance-level supervision is progressively introduced, providing flexibility and adaptability in the training. The pseudocode for self-annotating instance-level label is provided in Algorithm 1.

Once we have acquired the selected high attention instance-level embeddings across all bags, we concatenate them together to form all selected instances H'_{all} and their corresponding labels Y'_{all} . Then, H'_{all} and Y'_{all} are used to regularly train the instance-level classifier. In the attention-based frameworks [8, 9, 10, 11, 12], the attention network f_{attn} can simultaneously act as the instance-level classifier since the output attention map $A \in \mathbb{R}^{K \times \mathcal{N}}$ can be interpreted as the classification of instances, where \mathcal{N} denotes class number. Hence, in the instance-level branch, we optimise f_{attn} instead of the bag-level classifier.

To prove the instance-level learnability of CFSD, we follow the lemma D.1 and condition D.1 from Jang and Kwon. The proof is shown in Appendix D.2.

3.3 Contextual Encoding Generator (CEG)

To mitigate the limitations caused by the discontinuity instances in background-removed WSIs, we record the coordinates $(cx_k, cy_k) \in \mathbb{R}^{1 \times 2}$ for each valid instance, and concatenate them to be coordinates in a bag, denoted as $(\mathbf{cx}, \mathbf{cy}) \in \mathbb{R}^{K \times 2}$. Given the aspect ratios of WSIs vary, the coordinates are normalised within each bag, such that $(\mathbf{cx}', \mathbf{cy}') = \{(cx'_1, cy'_1), \dots, (cx'_k, cy'_k)\}$ with $cx'_k, cy'_k \in [0, 1]$. The \mathbf{cx} , \mathbf{cy} and the attention map A obtained from CFSD are together encoded to capture the contextual information:

$$\mathbf{h}_{pe} = \mathbf{h} + \varphi(\text{concat}(\text{sincos}(\mathbf{cx}'), \text{sincos}(\mathbf{cy}'), \text{sincos}(A))) \quad (6)$$

where \mathbf{h}_{pe} denotes the encoded feature, and φ is an MLP projector. The overview is shown in Figure 2 and pseudo-code is included in Algorithm 2.

3.4 LadderMIL

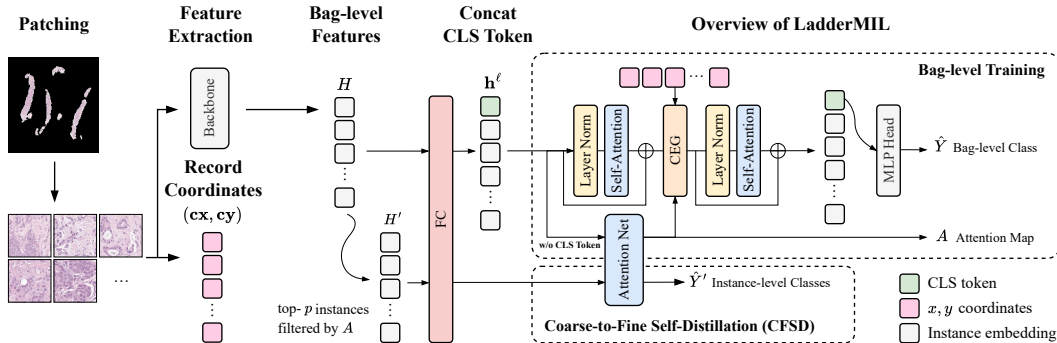


Figure 3: **Overview of the LadderMIL.** CLAM [9] is used to remove the background and a pre-trained backbone is used to extract features from each patch. (1) The embedded bag-level features are then processed by the bag-level branch to obtain the bag-level prediction \hat{Y} and attention map A . (2) Subsequently, the top- p instances in each bag are selected and assigned a label according to the bag-level label, to form an instance-level dataset H' with the corresponding labels Y' across all bags. (3) Next, these data are used to train the instance-level branch.

LadderMIL is a hybrid framework with CFSD and CEG, as shown in Figure 3. In the bag-level branch, we employ two transformer layers with self-attention and a CEG module located in between. Meanwhile, the bag level attention map A is obtained from the attention network f_{attn} . Building upon Eqn(2)(3)(5), and denoting the feature with CLS token as \mathbf{h}^ℓ and the bag-level prediction head as f_{cls} , the bag-level branch is composed as follow:

$$\mathbf{h} = \text{FC}(H), \quad A = f_{attn}(\mathbf{h}) \quad (7)$$

$$\hat{Y} = f_{cls}(f_{SA}(\text{CEG}(f_{SA}(\mathbf{h}, \mathbf{x}, \mathbf{y}, A)))) \quad (8)$$

while for classification tasks, the training is implemented following:

$$\mathcal{L}_{bag} = \text{CELoss}(\hat{Y}, Y) \quad (9)$$

Note that our method can be also applied for prognosis prediction, where the training is implemented following [19, 38]. The implementation details and loss function are shown in appendix F.

For the instance-level branch, CFSD is applied to facilitate instance-level learning. The instance-level branch is written as follows:

$$\hat{Y}' = f_{attn}(\mathbf{h}), \quad \mathcal{L}_{inst} = \text{CELoss}(\hat{Y}', Y') \quad (10)$$

By combining both branches, LadderMIL is trained by optimising the following objective:

$$\mathcal{L} = \mathcal{L}_{bag} + \mathcal{L}_{inst} \quad (11)$$

The implementation of LadderMIL in pseudo-code is described in Algorithm 3.

4 Experiments and Results

4.1 Tasks and Datasets

We evaluate the performance of LadderMIL on five clinically relevant tasks.

Breast Cancer Receptor Status Classification. The receptor status of estrogen receptor (ER) and progesterone receptor (PR) inform treatment decision making, while the classification is challenging since not all tumour cells in a sample are guaranteed to be of the same receptor status due to tumour cell hormone receptor heterogeneity. We perform hormone receptor status classification on our internal breast cancer dataset which consists of 491 clinical cases reported by expert consultant breast pathologists. The annotation protocol is described in Appendix E.

Prognosis Prediction. Prognosis prediction is a highly clinically relevant and challenging task. We evaluate prognosis prediction performance on the TCGA-LUAD dataset which contains 465 cases with readily available follow-up clinical data including survival months and censorship.

Subtype Classification. The capability of subtype classification is evaluated on the TCGA-RCC dataset, a kidney cancer dataset that contains three types of kidney cancer, including KIRC, KICH, and KIRP. After removing corrupted slides, the dataset consists of 919 diagnostic slides, with 517, 107, and 295 cases of the three subtypes, respectively.

Tumour Classification. The capability of tumour classification is evaluated on the CAMELYON16 dataset, which is focused on tumour lymph node metastasis versus normal node classification in breast cancer. It consists of 270 training cases (160 normal and 110 tumour), and 130 test cases.

4.2 Baseline Models

To demonstrate the superior performance of our framework, we compared LadderMIL with several baseline models, including the basic max-pooling and mean-pooling, ABMIL that utilises an attention-based pooling module [8], the popular CLAM-SB and CLAM-MB [9], AdditiveMIL [39] and SCLWC [11] that use gated attention, DSMIL [10] that applies dual-stream MIL with instance and bag

classifiers, and TransMIL [14] that applies PPEG and Nyström-Attention. It is important to note that SimCLR [40], a self-supervised contrastive learning method, was originally used to pre-train a ResNet-18 as the feature extractor for DSMIL. However, we omitted this step in our benchmarking as we aimed to compare the performance of the MIL frameworks rather than different feature extractors.

Additionally, we specifically compared our CFSD with WENO [18] by evaluating the combination of ABMIL+CFSD and DSMIL+CFSD, then comparing the performance gaps with those of vanilla ABMIL and DSMIL. Then, we used these performance gaps to benchmark with the results of ABMIL+WENO and DSMIL+WENO, as reported in their original paper.

4.3 Implementations

Preprocessing. We applied a consistent preprocessing protocol across all datasets, without data curation or normalisation, to better demonstrate our method’s robustness to staining and scanning variation. WSIs were standardised to 0.2631 microns per pixel (MPP) and patched at $20\times$ magnification. Background removal and patching were performed using CLAM [9] and OpenSlide [41], extracting non-overlapping patches of size 256×256 .

Feature extraction. We evaluated our method on features from two backbones. (1) Following the published prior work [30, 19, 39], we used an ImageNet pre-trained ResNet-50 [42] as a backbone, while embeddings were taken from the third layer, mean-pooled to obtain 1×1024 instance-level features, and concatenated to form the bag-level feature $H \in \mathbb{R}^{K \times 1024}$. (2) To further evaluate the generalisability, we also trained and evaluated on features extracted by GigaPath [31], a foundation model pre-trained on histopathology data, for receptor status classification and prognosis prediction tasks. The instance-level feature dimension for GigaPath is 1×1536 .

Experiment settings. For evaluation, we used the area under the curve (AUC) and F1-score as performance metrics for classification tasks, while the concordance index (C-index) is used to measure prognosis prediction performance. We rigorously employed five-fold cross-validation for the training of all tasks. For our internal dataset, TCGA-RCC, and TCGA-LUAD datasets, we split the data into a train:val:test ratio of 3:1:1, reporting the average metrics on the test set. For the CAMELYON16 dataset, we divided the training data into a train:val ratio of 4:1 for five-fold cross-validation and evaluated the model on the official test set, with the average metrics from the test set reported.

Training details. All experiments were undertaken on an RTX 3060 GPU. We used cross-entropy loss for both bag-level and instance-level training, with the AdamW optimiser [43] and CosineAnnealing [44] scheduler for optimisation. The learning rate was set to 2×10^{-4} with batch size of 1, while gradient accumulation was set to 32. We trained a total of 150 epochs, with early stopping applied if the metrics did not improve over 15 consecutive epochs. For fair comparison, we used the Lookahead optimiser [45] for TransMIL, adhering to their original design. For our LadderMIL, we first trained the bag-level network until it converged, and then applied CFSD to further train the bag-level and instance-level in a parallel way.

4.4 Results

The models trained with ResNet-50 extracted features are compared in Table 1. It is demonstrated that LadderMIL achieved significant performance improvements over the baseline models on all benchmarks, with AUC scores of 0.9178 and 0.8472 for ER and PR receptor status classification, respectively, an AUC of 0.9934 for subtype classification, an AUC of 0.8654 for tumour classification, and a C-index of 0.6096 for prognosis prediction.

On average, LadderMIL obtained improvements of 8.1%, 11%, and 2.4% in AUC, F1-score, and C-index, respectively, across the five benchmarks compared to the best baseline. Among the baselines, attention-based frameworks such as CLAM-SB, AdditiveMIL, and SCL-WC generally outperformed the others. In contrast, DSMIL showed limited performance due to the absence of SimCLR pre-trained features, highlighting a lack of robustness. Similarly, TransMIL underperformed in the training scheme using Lookahead optimiser that followed their original design, even compared to models without positional encoding. We attribute this to the susceptibility of PPEG to instance discontinuity, hindering its ability to capture true contextual relationships.

Table 1: **Model comparison on ResNet-50 extracted features.** **Bold** indicates overall the best while underline indicates the best in subgroup.

Dataset & Metrics	ER		PR		TCGA-RCC		CAMELYON16		TCGA-LUAD
	AUC	F1-score	AUC	F1-score	AUC	F1-score	AUC	F1-score	
MeanPooling	0.6458	0.5518	0.6482	0.5780	0.9558	0.8040	0.6194	0.5650	0.5400
MaxPooling	0.6560	0.5490	0.6488	0.5474	0.9650	0.8502	0.6756	0.6050	0.4964
ABMIL	0.6510	0.5572	0.6078	0.5458	0.9750	0.8430	0.6206	0.5838	<u>0.5952</u>
CLAM-SB	<u>0.8658</u>	0.7202	0.6656	0.6014	0.9838	0.8944	<u>0.7552</u>	<u>0.6592</u>	0.5396
CLAM-MB	0.8370	0.6946	0.7070	0.6092	0.9842	0.8894	0.7266	0.6500	0.5298
DSMIL	0.6794	0.5576	0.6204	0.5982	0.9716	0.8596	0.6342	0.6046	0.5706
TransMIL	0.6606	0.5576	0.6142	0.5544	<u>0.9850</u>	0.8860	0.6254	0.5676	0.5050
AdditiveMIL	0.8602	<u>0.7252</u>	0.6936	0.6300	0.9840	<u>0.8948</u>	0.7390	0.6410	0.5396
SCL-WC	0.8442	0.6972	<u>0.7616</u>	<u>0.6620</u>	0.9828	0.8920	0.7104	0.6428	0.5704
LadderMIL (Ours)	0.9178	0.7848	0.8472	0.7590	0.9924	0.9302	0.8654	0.7722	0.6096

Additionally, models trained on GigaPath-extracted features were evaluated on the challenging receptor status classification and prognosis prediction tasks, and compared in Table 2. Our LadderMIL continued to outperform other baselines, achieving up to a 3% improvement in prognosis prediction, further demonstrating its generalisability.

We also benchmarked our CFSD with the other knowledge distillation method *i.e.*, WENO. In the comparison between WENO and CFSD, we focus on the performance gap rather than the absolute performance, in order to mitigate the influence of differences in data splitting and hyperparameter settings. As shown in Table 3, CFSD significantly outperformed WENO on both ResNet-50 and GigaPath features, achieving the highest AUC improvements of 0.1486 and 0.2888 for ABMIL and DSMIL, respectively.

Table 2: **Model comparison on GigaPath extracted features.** **Bold** indicates overall the best while underline indicates the best in subgroup.

Dataset & Metrics	Internal (ER)		Internal (PR)		TCGA-LUAD
	AUC	F1	AUC	F1	
MeanPooling	0.8636	0.7040	0.8264	0.7296	0.5846
MaxPooling	0.8578	0.6666	0.7652	0.6798	0.4978
ABMIL	0.9216	0.7926	0.8452	<u>0.7572</u>	0.5558
CLAM-SB	0.9272	0.7752	0.8500	0.7310	0.5940
CLAM-MB	0.9280	0.8030	0.8572	0.7494	0.5638
DSMIL	0.9008	0.7636	0.8418	0.7524	0.5994
TransMIL	0.8876	0.7386	0.8318	0.7354	0.6030
AdditiveMIL	0.9272	0.7752	0.8500	0.7310	0.5940
SCL-WC	0.9220	0.7868	0.8530	0.7376	0.6108
LadderMIL (Ours)	0.9522	0.8186	0.8644	0.7612	0.6332

Table 3: **Comparing CFSD and WENO on CAMELYON16.** The performance gap Δ versus the vanilla model in AUC score is reported. Note that the Δ WENO is directly referenced from the original paper [18].

Models	ABMIL		DSMIL	
Metric	AUC		AUC	
Features	ResNet-50	GigaPath	ResNet-50	GigaPath
\times	0.6206	0.9432	0.6342	0.6670
CFSD	0.7692	0.9774	0.7562	0.9558
Δ CFSD	+0.1486	+0.0342	+0.1220	+0.2888
Δ WENO	+0.0284		+0.0094	

4.5 Ablation Study

Efficacy of CFSD and CEG. We next assessed the effectiveness of CFSD and CEG in Table 4. The results demonstrate that CFSD leads to obvious improvements in the attention-based framework of CLAM-SB. This highlights that enhancing learnability at the instance level is empirically beneficial to bag-level learning. Additionally, we show that the efficacy of CEG is substantial. LadderMIL with CEG outperforms the combinations with other positional encoding modules measured by both AUC, F1-score, and C-index, including PPEG. This improvement is attributed to the encoding of the accurate coordinates with the bag-level attention map, which better captures inter-instance contextual information in background-removed WSI. Full tables are shown in Appendix G.1.

Table 4: **Ablation study of CFSD and CEG on ResNet-50 extracted features.** **Bold** indicates overall the best while underline indicates the best in subgroup. C-index is reported for TCGA-LUAD while AUC is reported for others.

Framework	CFSD	PE	ER	PR	TCGA-RCC	CAMELYON16	TCGA-LUAD
CLAM-SB	×	×	0.8658	0.6656	0.9838	0.7552	0.5396
	✓	×	<u>0.8688</u>	<u>0.8150</u>	<u>0.9880</u>	<u>0.8472</u>	<u>0.5996</u>
LadderMIL (Ours)	×	Random	0.8588	0.7186	0.9880	0.8056	0.5716
	×	1D	0.8858	0.6362	0.9870	0.8448	0.5194
	×	2D	0.8906	0.8038	0.9864	0.7866	0.5908
	×	PPEG	0.8962	0.7756	0.9868	0.8260	0.5888
	✓	2D	0.9136	0.8432	0.9882	0.8594	0.5974
	✓	PPEG	0.9056	0.8274	0.9920	0.8588	0.6092
	✓	CEG	0.9178	0.8472	0.9924	0.8654	0.6096

Efficacy of ATS. The performance of LadderMIL with fixed top- p settings, including top-5%, top-10% and top-15%, was compared with the ATS applied counterparts in receptor classification. It is shown in Table 16 that ATS succeeded in flexibly adjusting the top- p threshold during training and introduced better performance.

Table 5: **Comparison of bag-level performance P_{bag} and instance-level P_{inst} performance for CFSD on the synthetic MNIST dataset.** The framework of CLAM-SB (baseline) and the CFSD plugged-in counterparts are tested.

Modules	P_{bag}		P_{inst}	
	AUC	F1-score	AUC	F1-score
×	0.9240	0.7346	0.4755	0.0659
✓	0.9254	0.7550	0.8645	0.4016

Table 6: **Training time compared on the ER classification training set with 239 cases.**

Models	Params.	Time/Epoch (s)	Gap vs. Ours
MeanPooling	2.05K	1.97	-0.74
MaxPooling	2.05K	1.9	-0.81
ABMIL	0.26M	2.07	-0.64
CLAM-SB	0.79M	2.31	-0.40
CLAM-MB	0.79M	2.35	-0.36
DSMIL	0.15M	2.73	+0.02
AdditiveMIL	0.79M	2.1	-0.61
SCL-WC	0.92M	2.27	-0.44
TransMIL	2.67M	3.88	+1.17
LadderMIL (Ours)	3.28M	2.71	0.00

Empirical proof of instance-level learnability. Furthermore, we demonstrate instance-level learnability using the synthetic MNIST dataset [46], following the approach outlined by Jang and Kwon. As shown in Table 5, the CLAM-SB baseline shows limited performance in instance-level classification. In contrast, CFSD is empirically proven to enable instance-level learning. The detailed implementation and full table are shown in Appendix D.3.

Training efficiency. We also analysed the training efficiency of LadderMIL versus other baselines. For epoch-wise training time (Table 6, full table in Appendix G.5), TransMIL takes a longer time in each epoch than LadderMIL. Combining the aforementioned results, LadderMIL brings distinct performance improvements versus other models, while limiting the maximum epoch-wise training time gap to only around 0.8s.

4.6 Interpretability

To assess the interpretability of LadderMIL, we visualised attention heatmaps for ER+ cases from our internal cohort, as shown in Appendix H. Immunohistochemistry (IHC) is the clinical gold standard for determining receptor status that uses antibody staining to detect antigens in tissue samples [47]. In IHC, brown staining indicates ER+ cells. By comparing the heatmaps with the IHC references, we find that regions of high attention align closely with brown-stained areas, suggesting the classification decisions of LadderMIL are clinically interpretable and capture relevant biological features.

5 Conclusion

In this paper, we propose LadderMIL, a novel framework that integrates the coarse-to-fine self-distillation (CFSD) paradigm and the contextual encoding generator (CEG) for multiple instance learning (MIL). CFSD enables efficient instance-level supervision by probing and distilling a classifier trained with bag-level labels, thereby addressing the limited instance-level learnability of MIL in a self-improving manner. Meanwhile, CEG mitigates issues arising from the discontinuity of instances

in background-removed WSIs and enhances the use of inter-instance contextual information by encoding precise coordinates and the bag-level attention map. The overall framework aligns with the decision-making and reasoning processes of pathologists, who assess both bag-level and instance-level features in parallel. By incorporating CFSD and CEG, LadderMIL outperforms state-of-the-art frameworks, while demonstrating instance-level learnability and interpretability.

Limitations. While the efficacy of CFSD and CEG has been demonstrated in our experimental setting, it will be crucial to explore how this method performs under different magnifications of WSI as well as under a wider range of clinically relevant tasks. Moreover, it would be valuable to investigate whether more advanced techniques, such as cross-attention [48], can be leveraged for multi-scale learning with instances across various magnifications. Taking the overlays shown in our framework, we hope this work will inspire future research aimed at developing a more universally applicable MIL architecture.

Broader Impact. MIL is a fundamental technique in computational pathology research, where researchers are not only looking for solutions to morphological tasks such as tumour detection but also hope to use deep learning to discover new knowledge in treatment response prediction [3, 37, 49] and prognosis prediction [4, 12, 19, 50, 51] by analysing whole-slide images. Our LadderMIL reveals an applicable method for reasonable knowledge discovery, since no prior knowledge has been introduced and instead the model improves itself cross-referencing the learned information from bag-level branch and instance-level branch.

References

- [1] Muhammad Khalid Khan Niazi, Anil V Parwani, and Metin N Gurcan. Digital pathology and artificial intelligence. *The Lancet Oncology*, 20(5):e253–e261, 2019.
- [2] Dehai Zhang, Yongchun Duan, Jing Guo, Yaowei Wang, Yun Yang, Zhenhui Li, Kelong Wang, Lin Wu, and Minghao Yu. Using multi-scale convolutional neural network based on multi-instance learning to predict the efficacy of neoadjuvant chemoradiotherapy for rectal cancer. *IEEE Journal of Translational Engineering in Health and Medicine*, 10:1–8, 2022.
- [3] Pegah Khosravi, Elizabeth J. Sutton, Justin Jee, Timothy Dalfonso, Christopher J. Fong, Doori Rose, Edaise M. Da Silva, Armaan Kohli, David Joon Ho, Mehnaj S. Ahmed, Danny Martinez, Anika Begum, Elizabeth Zakszewski, Andrew Aukerman, Yanis Tazi, Katja Pinker-Domenig, Sarah Eskreis-Winkler, Atif J. Khan, Edi Brogi, Elizabeth Morris, Sarat Chandarlapaty, George Plitas, Simon Powell, Monica Morrow, Larry Norton, Jianjiong Gao, Mark Robson, Hong Zhang, Sohrab Shah, Pedram Razavi, and MSK-MIND Consortium. Prediction of neoadjuvant treatment outcomes with multimodal data integration in breast cancer. *Cancer Research*, 82 (12_Supplement):1928–1928, 6 2022.
- [4] Junhao Liang, Weisheng Zhang, Jianghui Yang, Meilong Wu, Qionghai Dai, Hongfang Yin, Ying Xiao, and Lingjie Kong. Deep learning supported discovery of biomarkers for clinical prognosis of liver cancer. *Nature Machine Intelligence*, 5:408–420, 2023.
- [5] Zheng Gao, Tiandong Chen, and Bei Yang. A weakly supervised multiple instance learning approach for classification of Breast cancer HER-2 status using whole slide images. In *Third International Conference on Biomedical and Intelligent Systems*, volume 13208, page 132081D, 2024.
- [6] Chetan L. Srinidhi, Ozan Ciga, and Anne L. Martel. Deep neural network models for computational histopathology: A survey. *Medical Image Analysis*, 67:101813, 2021.
- [7] Thomas G. Dietterich, Richard H. Lathrop, and Tomás Lozano-Pérez. Solving the multiple instance problem with axis-parallel rectangles. *Artificial Intelligence*, 89(1):31–71, 1997.
- [8] Maximilian Ilse, Jakub M. Tomczak, and Max Welling. Attention-based deep multiple instance learning. In *Proceedings of the 35th International Conference on Machine Learning*, pages 2127–2136, 2018.

- [9] Ming Y. Lu, Drew F. K. Williamson, Tiffany Y. Chen, Richard J. Chen, Matteo Barbieri, and Faisal Mahmood. Data-efficient and weakly supervised computational pathology on whole-slide images. *Nature Biomedical Engineering*, 5(6):555–570, 2021.
- [10] Bin Li, Yin Li, and Kevin W Eliceiri. Dual-stream multiple instance learning network for whole slide image classification with self-supervised contrastive learning. In *Proceedings of the IEEE/CVF Conference on Computer Vision and Pattern Recognition*, pages 14318–14328, 2021.
- [11] Xiyue Wang, Jinxi Xiang, Jun Zhang, Sen Yang, Zhongyi Yang, Ming-Hui Wang, Jing Zhang, Wei Yang, Junzhou Huang, and Xiao Han. Sc-wc: Cross-slide contrastive learning for weakly-supervised whole-slide image classification. In *Advances in Neural Information Processing Systems*, 2022.
- [12] Richard J. Chen, Ming Y. Lu, Jingwen Wang, Drew F. K. Williamson, Scott J. Rodig, Neal I. Lindeman, and Faisal Mahmood. Pathomic fusion: An integrated framework for fusing histopathology and genomic features for cancer diagnosis and prognosis. *IEEE Transactions on Medical Imaging*, 41(4):757–770, 2022.
- [13] Alexey Dosovitskiy, Lucas Beyer, Alexander Kolesnikov, Dirk Weissenborn, Xiaohua Zhai, Thomas Unterthiner, Mostafa Dehghani, Matthias Minderer, Georg Heigold, Sylvain Gelly, Jakob Uszkoreit, and Neil Houlsby. An image is worth 16x16 words: Transformers for image recognition at scale. In *International Conference on Learning Representations*, 2021.
- [14] Zhuchen Shao, Hao Bian, Yang Chen, Yifeng Wang, Jian Zhang, Xiangyang Ji, and Yongbing Zhang. Transmil: Transformer based correlated multiple instance learning for whole slide image classification. In *Advances in Neural Information Processing Systems*, 2021.
- [15] Yunlong Zhang, Honglin Li, Yuxuan Sun, Sunyi Zheng, Chenglu Zhu, and Lin Yang. Attention-challenging multiple instance learning for whole slide image classification, 2023.
- [16] Jaeseok Jang and Hyuk-Yoon Kwon. Are multiple instance learning algorithms learnable for instances? In *Advances in Neural Information Processing Systems*, 2024.
- [17] Geoffrey Hinton, Oriol Vinyals, and Jeff Dean. Distilling the knowledge in a neural network. *arXiv preprint arXiv:1503.02531*, 2015.
- [18] Linhao Qu, xiaoyuan Luo, Manning Wang, and Zhijian Song. Bi-directional weakly supervised knowledge distillation for whole slide image classification. In *Advances in Neural Information Processing Systems*, 2022.
- [19] Richard J. Chen, Ming Y. Lu, Drew F.K. Williamson, Tiffany Y. Chen, Jana Lipkova, Zahra Noor, Muhammad Shaban, Maha Shady, Mane Williams, Bumjin Joo, and Faisal Mahmood. Pan-cancer integrative histology-genomic analysis via multimodal deep learning. *Cancer Cell*, 40(8):865–878.e6, 2022.
- [20] Carina Kludt, Yuan Wang, Waleed Ahmad, Andrey Bychkov, Junya Fukuoka, Nadine Gaisa, Mark Kühnel, Danny Jonigk, Alexey Pryalukhin, Fabian Mairinger, Franziska Klein, Anne Maria Schultheis, Alexander Seper, Wolfgang Hulla, Johannes Brägelmann, Sebastian Michels, Sebastian Klein, Alexander Quaas, Reinhard Büttner, and Yuri Tolkach. Next-generation lung cancer pathology: Development and validation of diagnostic and prognostic algorithms. *Nature Communication*, 5:101697, 2024.
- [21] Quanhao He, Bangxin Xiao, Yiwen Tan, Jun Wang, Hao Tan, Canjie Peng, Bing Liang, Youde Cao, and Mingzhao Xiao. Integrated multicenter deep learning system for prognostic prediction in bladder cancer. *npj Precision Oncology*, 8:233, 2024.
- [22] Xiangmin Han, Huijian Zhou, Zhiqiang Tian, Shaoyi Du, and Yue Gao. Inter-intra hypergraph computation for survival prediction on whole slide images. *IEEE Transactions on Pattern Analysis and Machine Intelligence*, pages 1–17, 2025.

- [23] Man M. Ho, Shikha Dubey, Yosep Chong, Beatrice Knudsen, and Tolga Tasdizen. F2fldm: Latent diffusion models with histopathology pre-trained embeddings for unpaired frozen section to ffpe translation. In *IEEE/CVF Winter Conference on Applications of Computer Vision*, pages 4382–4391, 2025.
- [24] Ashish Vaswani, Noam Shazeer, Niki Parmar, Jakob Uszkoreit, Llion Jones, Aidan N. Gomez, Łukasz Kaiser, and Illia Polosukhin. Attention is all you need. In *Advances in Neural Information Processing Systems*, 2017.
- [25] Xiangxiang Chu, Zhi Tian, Bo Zhang, Xinlong Wang, and Chunhua Shen. Conditional positional encodings for vision transformers. In *Proceedings of the 11th International Conference on Learning Representations*, 2023.
- [26] Kangning Liu, Weicheng Zhu, Yiqiu Shen, Sheng Liu, Narges Razavian, Krzysztof J Geras, and Carlos Fernandez-Granda. Multiple instance learning via iterative self-paced supervised contrastive learning. In *Proceedings of the IEEE/CVF Conference on Computer Vision and Pattern Recognition*, 2023.
- [27] Tiancheng Lin, Zhimiao Yu, Hongyu Hu, Yi Xu, and Chang-Wen Chen. Interventional bag multi-instance learning on whole-slide pathological images. In *Proceedings of the IEEE/CVF Conference on Computer Vision and Pattern Recognition*, 2023.
- [28] Wentao Huang, Xiaoling Hu, Shahira Abousamra, Prateek Prasanna, and Chao Chen. Hard negative sample mining for whole slide image classification. In *Medical Image Computing and Computer Assisted Intervention – MICCAI 2024*, pages 144–154, 2024.
- [29] Xiyue Wang, Sen Yang, Jun Zhang, Minghui Wang, Jing Zhang, Junzhou Huang, Wei Yang, and Xiao Han. Transpath: Transformer-based self-supervised learning for histopathological image classification. In *Proceedings of the International Conference on Medical Image Computing and Computer-Assisted Intervention*, pages 186–195, 2021.
- [30] Xiyue Wang, Sen Yang, Jun Zhang, Minghui Wang, Jing Zhang, Wei Yang, Junzhou Huang, and Xiao Han. Transformer-based unsupervised contrastive learning for histopathological image classification. *Medical Image Analysis*, 2022.
- [31] Hanwen Xu, Naoto Usuyama, Jaspreet Bagga, Sheng Zhang, Rajesh Rao, Tristan Naumann, Cliff Wong, Zelalem Gero, Javier González, Yu Gu, Yanbo Xu, Mu Wei, Wenhui Wang, Shuming Ma, Furu Wei, Jianwei Yang, Chunyuan Li, Jianfeng Gao, Jaylen Rosemon, Tucker Bower, Soohee Lee, Roshanthi Weerasinghe, Bill J. Wright, Ari Robicsek, Brian Piening, Carlo Bifulco, Sheng Wang, and Hoifung Poon. A whole-slide foundation model for digital pathology from real-world data. *Nature*, 2024.
- [32] Richard J. Chen, Tong Ding, Ming Y. Lu, Drew F. K. Williamson, Guillaume Jaume, Andrew H. Song, Bowen Chen, Andrew Zhang, Daniel Shao, Muhammad Shaba, Mane Williams, Lukas Oldenburg, Luca L. Weishaupt, Judy J. Wang, Anurag Vaidya, Long Phi Le, Georg Gerber, Sharifa Sahai, Walt Williams, and Faisal Mahmood. Towards a general-purpose foundation model for computational pathology. *Nature Medicine*, 30:850–862, 2024.
- [33] Eugene Vorontsov, Alican Bozkurt, Adam Casson, George Shaikovski, Michal Zelechowski, Kristen Severson, Eric Zimmermann, James Hall, Neil Tenenholtz, Nicolo Fusi, Ellen Yang, Philippe Mathieu, Alexander van Eck, Donghun Lee, Julian Viret, Eric Robert, Yi Kan Wang, Jeremy D. Kunz, Matthew C. H. Lee, Jan H. Bernhard, Ran A. Godrich, Gerard Oakley, Ewan Millar, Matthew Hanna, Hannah Wen, Juan A. Retamero, William A. Moye, Razik Yousfi, Christopher Kanan, David S. Klimstra, Brandon Rothrock, Siqi Liu, and Thomas J. Fuchs. A foundation model for clinical-grade computational pathology and rare cancers detection. *Nature Medicine*, 30:2429–2935, 2024.
- [34] Hongrun Zhang, Yanda Meng, Yitian Zhao, Yihong Qiao, Xiaoyun Yang, Sarah E. Coupland, and Yalin Zheng. Dtfd-mil: Double-tier feature distillation multiple instance learning for histopathology whole slide image classification. In *Proceedings of the IEEE/CVF Conference on Computer Vision and Pattern Recognition*, pages 18780–18790, 2022.

- [35] Guillaume Jaume, Paul Doucet, Andrew H. Song, Ming Y. Lu, Cristina Almagro-Pérez, Sophia J. Wagner, Anurag J. Vaidya, Richard J. Chen, Drew F.K. Williamson, Ahrong Kim, and Faisal Mahmood. Hest-1k: A dataset for spatial transcriptomics and histology image analysis. In *Advances in Neural Information Processing Systems*, 2024.
- [36] Yunyang Xiong, Zhanpeng Zeng, Rudrasis Chakraborty, Mingxing Tan, Glenn Fung, Yin Li, and Vikas Singh. Nyströmformer: A nyström-based algorithm for approximating self-attention. In *Proceedings of the 35th Conference on Artificial Intelligence (AAAI-21)*, 2021.
- [37] Kang-Bo Huang, Cheng-Peng Gui, Yun-Ze Xu, Xue-Song Li, Hong-Wei Zhao, Jia-Zheng Cao, Yu-Hang Chen, Yi-Hui Pan, Bing Liao, Yun Cao, Xin-Ke Zhang, Hui Han, Fang-Jian Zhou, Ran-Yi Liu, Wen-Fang Chen, Ze-Ying Jiang, Zi-Hao Feng, Fu-Neng Jiang, Yan-Fei Yu, Sheng-Wei Xiong, Guan-Peng Han, Qi Tang, Kui Ouyang, Gui-Mei Qu, Ji-Tao Wu, Ming Cao, Bai-Jun Dong, Yi-Ran Huang, Jin Zhang, Cai-Xia Li, Pei-Xing Li, Wei Chen, Wei-De Zhong, Jian-Ping Guo, Zhi-Ping Liu, Jer-Tsong Hsieh, Dan Xie, Mu-Yan Cai, Wei Xue, Jin-Huan Wei, and Jun-Hang Luo. A multi-classifier system integrated by clinico-histology-genomic analysis for predicting recurrence of papillary renal cell carcinoma. *Nature Communication*, 15:6215, 2024.
- [38] Shekoufeh Gorgi Zadeh and Matthias Schmid. Bias in cross-entropy-based training of deep survival networks. *IEEE Transactions on Pattern Analysis and Machine Intelligence*, 43(9): 3126–3137, 2021.
- [39] Syed Ashar Javed, Dinkar Juyal, Harshith Padigela, Amaro Taylor-Weiner, Limin Yu, and aaditya prakash. Additive MIL: Intrinsically interpretable multiple instance learning for pathology. In *Advances in Neural Information Processing Systems*, 2022.
- [40] Ting Chen, Simon Kornblith, Mohammad Norouzi, and Geoffrey Hinton. A simple framework for contrastive learning of visual representations. In *Proceedings of the 37th International Conference on Machine Learning*, 2020.
- [41] Adam Goode, Benjamin Gilbert, Jan Harkes, Drazen Jukic, and Mahadev Satyanarayanan. Openslide: A vendor-neutral software foundation for digital pathology. *Journal of Pathology Informatics*, 4(1):27, 2013.
- [42] Kaiming He, Xiangyu Zhang, Shaoqing Ren, and Jian Sun. Deep residual learning for image recognition. In *Proceedings of the IEEE/CVF Conference on Computer Vision and Pattern Recognition (CVPR)*, 2016.
- [43] Ilya Loshchilov and Frank Hutter. Decoupled weight decay regularization. In *Proceedings of the International Conference on Learning Representations*, 2019.
- [44] Ilya Loshchilov and Frank Hutter. SGDR: Stochastic gradient descent with warm restarts. In *Proceedings of the International Conference on Learning Representations*, 2017.
- [45] Michael R. Zhang, James Lucas, Geoffrey Hinton, and Jimmy Ba. Lookahead optimizer: k steps forward, 1 step back. In *Advances in Neural Information Processing Systems*, 2019.
- [46] Li Deng. The mnist database of handwritten digit images for machine learning research [best of the web]. *IEEE Signal Processing Magazine*, 29(6):141–142, 2012.
- [47] R A Walker. Immunohistochemical markers as predictive tools for breast cancer. *Journal of Clinical Pathology*, 61(6):689–696, 2008.
- [48] Chun-Fu (Richard) Chen, Quanfu Fan, and Rameswar Panda. CrossViT: Cross-Attention Multi-Scale Vision Transformer for Image Classification. In *Proceedings of the International Conference on Computer Vision*, 2021.
- [49] Xiaodong Wang, Ying Chen, Yunshu Gao, Huiqing Zhang, Zehui Guan, Zhou Dong, Yuxuan Zheng, Jiarui Jiang, Haoqing Yang, Liming Wang, Xianming Huang, Lirong Ai, Wenlong Yu, Hongwei Li, Changsheng Dong, Zhou Zhou, Xiyang Liu, and Guanzhen Yu. Predicting gastric cancer outcome from resected lymph node histopathology images using deep learning. *Nature Communication*, 12:1637, 2021.

- [50] Xuejun Qian, Jing Pei, Chunguang Han, Zhiying Liang, Gaosong Zhang, Na Chen, Weiwei Zheng, Fanlun Meng, Dongsheng Yu, Yixuan Chen, Yiqun Sun, Hanqi Zhang, Wei Qian, Xia Wang, Zhuoran Er, Chenglu Hu, Hui Zheng, and Dinggang Shen. A multimodal machine learning model for the stratification of breast cancer risk. *Nature Biomedical Engineering*, 2024.
- [51] Sarah Volinsky-Fremont, Nanda Horeweg, Sonali Andani, Jurriaan Barkey Wolf, Maxime W. Lafarge, Cor D. de Kroon, Gitte Ørtoft, Estrid Høgdall, Jouke Dijkstra, Jan J. Jobsen, Ludy C. H. W. Lutgens, Melanie E. Powell, Linda R. Mileshekin, Helen Mackay, Alexandra Leary, Dionyssios Katsaros, Hans W. Nijman, Stephanie M. de Boer, Remi A. Nout, Marco de Bruyn, David Church, Vincent T. H. B. M. Smit, Carien L. Creutzberg, Viktor H. Koelzer, and Tjalling Bosse. Prediction of recurrence risk in endometrial cancer with multimodal deep learning. *Nature Medicine*, 30:1962–1973, 2024.
- [52] International Collaboration on Cancer Reporting. Invasive carcinoma of the breast, 2022. URL <https://www.iccr-cancer.org/datasets/published-datasets/breast/invasive-carcinoma-of-the-breast/>.
- [53] Babak Ehteshami Bejnordi, Mitko Veta, Paul Johannes van Diest, Bram van Ginneken, Nico Karssemeijer, Geert Litjens, Jeroen A. W. M. van der Laak, and the CAMELYON16 Consortium. Diagnostic assessment of deep learning algorithms for detection of lymph node metastases in women with breast cancer. *JAMA*, 318:2199–2210, 2017.

A Discontinuity between Patches

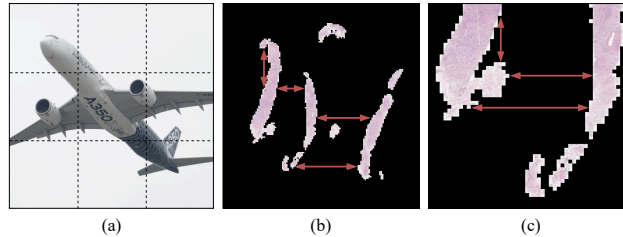
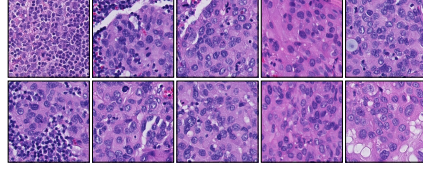


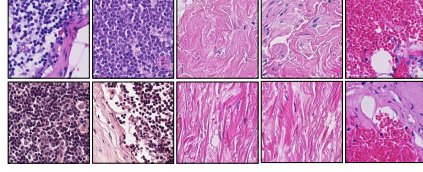
Figure 4: **A comparison shows the differences between the patching of ViT with ordinary square images and the patching of WSI.** (a) shows a square aircraft image, which typically processed by ViT that with minor discontinuity. The implementation of ViT splits it into fixed-size patches as the dash lines indicate. (b) shows a background removed WSI. (c) the a corresponding zoom-in view for better visualisation. The red arrows points out examples of discontinuous patches.

B Examples for Visulising Top- p Patches in Preliminary Experiment

In this experiment, we applied CLAM-SB [9], a model based on the framework of AMIL, to the CAMELYON16 benchmarking task. By comparing the instances with top- p importance and reverse top- p importance in the attention map A , we observed that CLAM-SB effectively focused on tumour instances (Figure 5). This result suggests that annotating high-attention instances with bag-level labels is reasonable and highlights the potential for using self-distillation learning with bag-level knowledge, laying the groundwork for instance-level supervision in MIL.



(a) Examples of top- p importance instances.



(b) Examples of reverse top- p importance instances.

Figure 5: **Instances visualisation of preliminary experiments.** In (a), we can see top- p instances contain tumour areas, while in (b) the reverse top- p instances contain mainly stroma, inflammatory cells, and red blood cells. The bag-level model can provide correct classification for top- p instances.

C Algorithms

Algorithm 1 Self-annotating instance-level label

Input: data H , target Y , attention map A
Output: inst_data H' , inst_target Y'
for each bag do
 1) argsort and rank attention score;
 $A_{\text{ranked}} \leftarrow \text{argsort}(A)/K$
 2) get top- p instances based on threshold th ;
 $\text{selected_idx} \leftarrow A_{\text{ranked}} > th \in [0.8, 0.95]$
 3) Get H' and Y' ;
 $H' \leftarrow H[\text{selected_idx}]$, $Y' \leftarrow Y$ repeat for $\text{len}(\text{selected_idx})$
end for
Given the bag number m :
 $H'_{\text{all}} \leftarrow \text{concat}(H'_1, H'_2, \dots, H'_m)$
 $Y'_{\text{all}} \leftarrow \text{concat}(Y'_1, Y'_2, \dots, Y'_m)$

Algorithm 2 Contextual Encoding Generator

Input: data with CLS token $\mathbf{h}^\ell \in \mathbb{R}^{(k+1) \times 512}$, coordinates $(\mathbf{cx}, \mathbf{cy})$, attention map A
Output: context encoded embeddings \mathbf{h}_{pe}^ℓ
1) Normalise coordinates;
for each $(\mathbf{cx}, \mathbf{cy})$ **do**
 $\text{max_scale} \leftarrow \max(\max(\mathbf{cx}), \max(\mathbf{cy}))$
 $(\mathbf{cx}', \mathbf{cy}') \leftarrow \text{min_max_scaler}(\mathbf{cx}, \mathbf{cy}, \text{max_scale})$
end for
2) Contextual encoding;
 $\mathbf{h}, \mathbf{h}^{\ell(0)} \leftarrow \mathbf{h}^\ell$, where $\mathbf{h}^{\ell(0)}$ is the CLS token that $\mathbf{h}^{\ell(0)} \in \mathbb{R}^{1 \times 512}$
 $\mathbf{h}_{pe} \leftarrow \mathbf{h} + \varphi(\text{concat}(\text{sincos}(\mathbf{cx}'), \text{sincos}(\mathbf{cy}'), \text{sincos}(A)))$, where φ is an MLP projector
 $\mathbf{h}_{pe}^\ell \leftarrow \text{concat}(\mathbf{h}_{pe}, \mathbf{h}^{\ell(0)})$

Algorithm 3 LadderMIL

Input: data H , coordinates $(\mathbf{cx}, \mathbf{cy})$
for each iteration **do**
 $\mathbf{h} \leftarrow \text{FC}(H)$, where $\mathbf{h} \in \mathbb{R}^{K \times 512}$
 if bag-level **then**
 $A \leftarrow f_{\text{attn}}(\mathbf{h})$
 $\mathbf{h}^\ell \leftarrow \text{concat}(\text{CLS}, \mathbf{h})$
 $\mathbf{h}' \leftarrow f_{SA}(\text{CEG}(f_{SA}(\mathbf{h}^\ell, \mathbf{x}, \mathbf{y}, A)))$
 $\mathbf{h}'' \leftarrow \text{layer_norm}(\mathbf{h}')^{(0)}$, where \mathbf{h}'' is the CLS token
 $\hat{Y} \leftarrow f_{cls}(\mathbf{h}'')$
 Output: \hat{Y}, A
 else if instance-level **then**
 $\hat{Y}' \leftarrow f_{\text{attn}}(\mathbf{h})$
 Output: \hat{Y}'
 end if
end for

D Instance-level Learnability

D.1 Lemma and Condition [16]

Given \mathcal{H} denotes the hypothesis space, \mathcal{H}_{inst_i} is the i^{th} instance hypothesis space, where $\mathcal{H}_{inst_i} = \{h_i : h_i(X_i) \rightarrow Y_i\}$. And \mathcal{H}_{add_i} is the extra hypothesis space from external values for the i^{th} instance. With $\mathcal{X} := \{\mathcal{X}_{inst_1}, \mathcal{X}_{inst_2}, \dots, \mathcal{X}_{inst_N}\}$ to be the bag-level feature space and $\mathcal{Y} := \{1, \dots, k\}$ to be the bag label space, we have:

Condition D.1. \mathcal{H}_{add_i} must be a subset of \mathcal{H}_{inst_i} that:

$$\mathcal{H}_{add_i} \subset \mathcal{H}_{inst_i} := \{h_{add_i} : \mathcal{X}_{add_i} \rightarrow \mathcal{Y}\} \quad (12)$$

Lemma D.1. Condition D.1 is a necessary condition for the learnability of instances, when the hypothesis space for the i^{th} instance of a MIL algorithm is $\mathcal{H}_{inst_i} \cup \mathcal{H}_{add_i}$, where \mathcal{H}_{inst_i} denotes the hypothesis space for the i^{th} instance and \mathcal{H}_{add_i} denotes the hypothesis space for the i^{th} instance generated through elements outside the i^{th} instance.

D.2 Theoretical proof of instance-level learnability

Proof. Given \mathcal{H}_{inst_k} and \mathcal{H}_{add_k} as the hypothesis space for the k^{th} instance and the hypothesis space for the k^{th} instance generated through elements outside of the k^{th} instance, respectively. The instance-level classifier in CFSD is denoted as $g(\cdot)$ and $f_{\mathcal{H}}$ denotes the individual hypothesis in corresponding hypothesis space \mathcal{H} . Hence we have:

$$G(h) = g_k(\mathbf{h}_k)$$

$$\mathcal{H}_{add_k} = \{f_{\mathcal{H}} : G(h) \rightarrow y_k\}$$

$$\mathcal{H}_{add_k} = \{f_{\mathcal{H},k} : g_k(\mathbf{h}_k) \rightarrow y_k\}$$

which obeys the pattern of \mathcal{H}_{inst_k} that produces results dependent solely on the k^{th} instance feature:

$$\mathcal{H}_{inst_k} = \{f_{\mathcal{H},k} : f_{\mathcal{H},k}(\mathbf{h}_k) \rightarrow y_k\}$$

The condition D.1 is satisfied that:

$$\mathcal{H}_{add_k} \subset \mathcal{H}_{inst_k}$$

and according to lemma D.1, CFSD is instance-level learnable. \square

D.3 Empirical proof of instance-level learnability

To demonstrate instance-level learnability, we followed the setup of Jang and Kwon using a synthetic MNIST dataset. The task is framed as a multi-class classification MIL problem, with bag-level labels assigned as shown in Table 7. To isolate the impact of CEG and given that the MNIST dataset lacks inherent positional information, we employed CLAM-SB (baseline) with CFSD to assess instance-level learnability, rather than using LadderMIL with positional encoding. Hyperparameters were set in accordance with our main experiments, except for the learning rate, which was adjusted to 0.001. The MNIST dataset was split into 80% training and 20% evaluation data. Performance was evaluated using one-vs-rest AUC and F1-score. In this experiment, we not only empirically demonstrated instance-level learnability but also validated the multi-class classification capability of our framework.

Table 7: **Annotation of the synthetic MNIST dataset.**

Bag-label	Description
3	the bag contains both 1 and 7
2	the bag contains 1 but not 7
1	the bag contains both 3 and 5
0	other combinations

Table 8: **Full table: Comparison of bag-level performance P_{bag} and instance-level P_{inst} performance for CFSD on the synthetic MNIST dataset.** The framework of CLAM-SB (baseline) and the CFSD plugged-in counterparts are tested in the experiment.

Modules	P_{bag}		P_{inst}		$P_{inst} - P_{bag}$	
CFSD	AUC	F1-score	AUC	F1-score	AUC	F1-score
×	0.9240	0.7346	0.4755	0.0659	-0.4485	-0.6687
✓	0.9254	0.7550	0.8645	0.4016	-0.0609	-0.3534

E Annotation Protocol for Receptor Status Classification

In clinical practice, both ER and PR are scored using a proportion score (PS) and an intensity score (IS), where $PS \in \mathbb{Z} \cap [0, 5]$ and $IS \in \mathbb{Z} \cap [0, 3]$. These scores are then combined to form a total score (TS), where $TS \in \mathbb{Z} \cap [0, 8]$, with $TS \neq 1$, and a higher score indicates greater receptor positivity. When converting into binary positive or negative status for classification, we take TS of 0 and 2 as negative, and TS from 3 to 8 as positive, in line with the clinical guideline [52]. Note that a $TS = 1$ does not exist, as either $PS = 0$ or $IS = 0$ would imply the absence of receptor expression.

F Implementation Details for Prognosis Prediction

F.1 Annotation Protocol

Following [12, 19], prognosis prediction is formalised as a four-class classification problem that splits patient survivorship into four discrete time slots. In preprocessing, to avoid data imbalance, data are distributed into four bins with equal cases number according to survival months using the `qcut` function from the pandas library. The annotation is made based the bin that the case is belonged to.

F.2 Loss Function

Under this formulation, patients have vital status (caused death) are considered as uncensored while patients alive are censored. β is a variable for adjusting the weight of censored and uncensored loss. Let Y_{hazard} and Y_{surv} denote the predicted risk and survival rate, respectively, the censored loss

$\mathcal{L}_{censored}$, uncensored loss $\mathcal{L}_{uncensored}$ and the loss for prognosis prediction \mathcal{L}_{surv} are defined as follow [19, 38]:

$$Y_{hazard} = \text{Sigmoid}(F_{bag}(\mathbf{h}, \mathbf{x}, \mathbf{y}, A)) \quad (13)$$

$$Y_{surv} = \prod (1 - Y_{hazard}) \quad (14)$$

$$\mathcal{L}_{censored} = -\log(Y_{surv}) \quad (15)$$

$$\mathcal{L}_{uncensored} = -\log(Y_{surv}) - \log(Y_{hazard}) \quad (16)$$

$$\mathcal{L}_{surv} = (1 - \beta)\mathcal{L}_{censored} + \beta\mathcal{L}_{uncensored} \quad (17)$$

G Supplementary Results

G.1 Ablation Study

Table 9: **Full table: Ablation study of CFSD and CEG on ResNet-50 extracted features.** Bold indicates overall the best while underline indicates the best in subgroup.

Framework	Modules		Internal (ER)		Internal (PR)		TCGA-RCC		CAMELYON16		TCGA-LUAD
	CFSD	PE	AUC	F1-score	AUC	F1-score	AUC	F1-score	AUC	F1-score	
CLAM-SB	×	×	0.8658	0.7202	0.6656	0.6014	0.9838	0.8944	0.7552	0.6592	0.5396
CLAM-SB	✓	×	<u>0.8688</u>	<u>0.7360</u>	<u>0.8150</u>	<u>0.7064</u>	<u>0.9880</u>	<u>0.9094</u>	<u>0.8472</u>	<u>0.7592</u>	<u>0.5996</u>
LadderMIL (Ours)	×	Random	0.8588	0.6982	0.7186	0.6800	0.9880	0.8966	0.8056	0.7162	0.5716
	×	1D	0.8858	0.7338	0.6362	0.5686	0.9870	0.9060	0.8448	0.7522	0.5194
	×	2D	0.8906	0.7656	0.8038	0.6998	0.9864	0.8950	0.7866	0.6948	0.5908
	×	PPEG	0.8962	0.7596	0.7756	0.6886	0.9868	0.8978	0.8260	0.7364	0.5888
	✓	2D	0.9136	0.7770	0.8432	0.7424	0.9882	0.9224	0.8594	0.7684	0.5974
	✓	PPEG	0.9056	0.7724	0.8274	0.7320	0.9920	0.9270	0.8588	0.7582	0.6092
	✓	CEG	0.9178	0.7848	0.8472	0.7590	0.9924	0.9302	0.8654	0.7722	0.6096

Table 10: **Full table: Ablation study of CFSD and CEG on GigaPath extracted features.** Bold indicates overall the best while underline indicates the best in subgroup.

Framework	Modules		Internal (ER)		Internal (PR)		TCGA-LUAD	
	CFSD	PE	AUC	F1-score	AUC	F1-score	C-index	
CLAM-SB	×	×	0.9272	0.7752	0.8500	0.7310	0.5940	
CLAM-SB	✓	×	<u>0.9438</u>	<u>0.8080</u>	<u>0.8550</u>	<u>0.7456</u>	<u>0.6280</u>	
LadderMIL (Ours)	×	Random	0.9106	0.7514	0.8530	0.7516	0.5996	
	×	1D	0.9318	0.8090	0.8510	0.7216	0.5466	
	×	2D	0.9308	0.7978	0.8550	0.7590	0.6162	
	×	PPEG	0.9016	0.7798	0.8510	0.7438	0.5794	
	✓	2D	0.9440	0.8072	0.8602	0.7584	0.6256	
	✓	PPEG	0.9458	0.8086	0.8590	0.7578	0.6264	
	✓	CEG	0.9522	0.8186	0.8644	0.7612	0.6332	

G.2 Standard Deviations

Table 11: **Standard deviations of model comparison on ResNet-50 extracted features.**

Dataset & Metrics	Internal (ER)		Internal (PR)		TCGA-RCC		CAMELYON16		TCGA-LUAD
	AUC	F1-score	AUC	F1-score	AUC	F1-score	AUC	F1-score	
MeanPooling	±0.0726	±0.0425	±0.0622	±0.0464	±0.0060	±0.0177	±0.0811	±0.0739	±0.0879
MaxPooling	±0.1418	±0.0773	±0.0675	±0.0815	±0.0126	±0.0301	±0.0375	±0.0235	±0.0504
ABMIL	±0.0540	±0.0445	±0.0857	±0.0694	±0.0072	±0.0697	±0.0953	±0.0706	±0.0610
CLAM-SB	±0.0491	±0.0688	±0.1204	±0.1108	±0.0065	±0.0271	±0.0476	±0.0271	±0.0493
CLAM-MB	±0.0457	±0.0554	±0.1218	±0.1226	±0.0061	±0.0289	±0.0659	±0.0562	±0.0362
DSMIL	±0.0713	±0.0364	±0.1082	±0.1035	±0.0040	±0.0197	±0.0771	±0.0807	±0.0630
TransMIL	±0.0949	±0.0648	±0.1080	±0.0639	±0.0073	±0.0256	±0.0995	±0.0828	±0.0916
AdditiveMIL	±0.0500	±0.0550	±0.1393	±0.1198	±0.0066	±0.0250	±0.0672	±0.0506	±0.0493
SCL-WC	±0.0629	±0.0560	±0.0651	±0.0784	±0.0070	±0.0239	±0.0441	±0.0355	±0.0520
LadderMIL (Ours)	±0.0270	±0.0589	±0.0636	±0.0738	±0.0034	±0.0155	±0.0458	±0.0386	±0.0450

Table 12: **Standard deviations of model comparison on GigaPath extracted features.**

Dataset & Metrics	Internal (ER)		Internal (PR)		TCGA-LUAD
	AUC	F1-score	AUC	F1-score	C-index
MeanPooling	± 0.0656	± 0.0605	± 0.0620	± 0.0727	± 0.0567
MaxPooling	± 0.0600	± 0.0841	± 0.0822	± 0.0681	± 0.0793
ABMIL	± 0.0334	± 0.0612	± 0.0646	± 0.0668	± 0.0806
CLAM-SB	± 0.0303	± 0.0440	± 0.0555	± 0.0388	± 0.0843
CLAM-MB	± 0.0252	± 0.0480	± 0.0523	± 0.0569	± 0.0468
DSMIL	± 0.0509	± 0.0757	± 0.0578	± 0.0549	± 0.1037
TransMIL	± 0.0385	± 0.0582	± 0.0699	± 0.0947	± 0.0762
AdditiveMIL	± 0.0303	± 0.0440	± 0.0555	± 0.0388	± 0.0843
SCL-WC	± 0.0312	± 0.0532	± 0.0604	± 0.0601	± 0.0724
LadderMIL (Ours)	± 0.0179	± 0.0449	± 0.0472	± 0.0526	± 0.0564

Table 13: **Standard deviations of ablation study on ResNet-50 extracted features.**

Framework	Modules		Internal (ER)		Internal (PR)		TCGA-RCC		CAMELYON16		TCGA-LUAD
	CFSD	PE	AUC	F1-score	AUC	F1-score	AUC	F1-score	AUC	F1-score	C-index
CLAM-SB	×	×	± 0.0414	± 0.0663	± 0.1204	± 0.1108	± 0.0065	± 0.0271	± 0.0476	± 0.0271	± 0.0493
CLAM-SB	✓	×	± 0.0500	± 0.0689	± 0.0417	± 0.0218	± 0.0065	± 0.0237	± 0.0495	± 0.0634	± 0.0432
LadderMIL (Ours)	×	Random	± 0.0410	± 0.0852	± 0.1429	± 0.1056	± 0.0044	± 0.0194	± 0.0529	± 0.0494	± 0.0391
	×	1D	± 0.0325	± 0.0355	± 0.1471	± 0.1138	± 0.0059	± 0.0150	± 0.0559	± 0.0390	± 0.0659
	×	2D	± 0.0508	± 0.0607	± 0.0461	± 0.0251	± 0.0047	± 0.0235	± 0.0726	± 0.0865	± 0.0557
	×	PPEG	± 0.0397	± 0.0519	± 0.0397	± 0.0393	± 0.0071	± 0.0124	± 0.0724	± 0.0561	± 0.0599
	✓	2D	± 0.0187	± 0.0410	± 0.0611	± 0.0682	± 0.0031	± 0.0191	± 0.0341	± 0.0359	± 0.0238
	✓	PPEG	± 0.0322	± 0.0634	± 0.0454	± 0.0331	± 0.0042	± 0.0240	± 0.0130	± 0.0200	± 0.0573
	✓	CEG	± 0.0270	± 0.0589	± 0.0636	± 0.0738	± 0.0034	± 0.0155	± 0.0458	± 0.0386	± 0.0450

Table 14: **Standard deviations of ablation study on GigaPath extracted features.**

Framework	Modules		Internal (ER)		Internal (PR)		TCGA-LUAD
	CFSD	PE	AUC	F1	AUC	F1	c-index
CLAM-SB	×	×	± 0.0303	± 0.0440	± 0.0555	± 0.0388	± 0.0843
CLAM-SB	✓	×	± 0.0164	± 0.0320	± 0.0561	± 0.0492	± 0.0591
LadderMIL (Ours)	×	Random	± 0.0464	± 0.0773	± 0.0583	± 0.0485	± 0.0737
	×	1D	± 0.0277	± 0.0557	± 0.0528	± 0.0580	± 0.0727
	×	2D	± 0.0294	± 0.0706	± 0.0507	± 0.0382	± 0.0949
	×	PPEG	± 0.0615	± 0.0691	± 0.0525	± 0.0474	± 0.0427
	✓	2D	± 0.0295	± 0.0653	± 0.0595	± 0.0597	± 0.0676
	✓	PPEG	± 0.0129	± 0.0437	± 0.0484	± 0.0506	± 0.0901
	✓	CEG	± 0.0179	± 0.0449	± 0.0472	± 0.0526	± 0.0564

G.3 Confidence Intervals

Table 15: **Confidence intervals for model comparison on ResNet-50 extract features.** Since we implemented five-fold cross-validation, the 95% CI for each split is separately reported in the table.

Task	Model	AUC Confidence Interval				
		Split 0	Split 1	Split 2	Split 3	Split 4
ER	MeanPooling	0.609-0.847	0.413-0.712	0.436-0.737	0.584-0.833	0.502-0.785
	MaxPooling	0.672-0.884	0.521-0.791	0.252-0.578	0.575-0.827	0.608-0.852
	ABMIL	0.516-0.788	0.543-0.806	0.424-0.728	0.601-0.843	0.486-0.773
	CLAM-SB	0.870-0.977	0.703-0.901	0.763-0.934	0.846-0.968	0.762-0.933
	CLAM-MB	0.796-0.946	0.686-0.891	0.713-0.910	0.833-0.963	0.720-0.913
	DSMIL	0.680-0.888	0.488-0.768	0.453-0.750	0.582-0.832	0.541-0.811
	TransMIL	0.397-0.699	0.546-0.808	0.490-0.776	0.711-0.905	0.495-0.779
	AdditiveMIL	0.870-0.977	0.702-0.900	0.740-0.923	0.834-0.963	0.761-0.933
	SCL-WC	0.862-0.974	0.684-0.890	0.700-0.903	0.846-0.968	0.707-0.906
	LadderMIL (Ours)	0.895-0.986	0.843-0.966	0.844-0.969	0.910-0.992	0.817-0.958
PR	MeanPooling	0.575-0.794	0.461-0.708	0.532-0.765	0.468-0.714	0.628-0.834
	MaxPooling	0.638-0.839	0.421-0.674	0.532-0.764	0.544-0.774	0.535-0.767
	ABMIL	0.421-0.670	0.408-0.662	0.483-0.726	0.483-0.726	0.650-0.849
	CLAM-SB	0.351-0.606	0.515-0.751	0.653-0.851	0.569-0.793	0.692-0.876
	CLAM-MB	0.735-0.901	0.538-0.769	0.392-0.648	0.655-0.853	0.700-0.881
	DSMIL	0.434-0.681	0.378-0.635	0.558-0.784	0.461-0.708	0.689-0.875
	TransMIL	0.598-0.811	0.313-0.573	0.599-0.814	0.466-0.712	0.510-0.748
	AdditiveMIL	0.351-0.606	0.515-0.752	0.655-0.852	0.731-0.900	0.697-0.879
	SCL-WC	0.779-0.926	0.603-0.817	0.580-0.801	0.668-0.861	0.700-0.881
	LadderMIL (Ours)	0.841-0.959	0.708-0.886	0.729-0.899	0.796-0.937	0.832-0.956
TCGA-RCC	MeanPooling	0.917-0.974	0.934-0.981	0.943-0.981	0.924-0.976	0.930-0.983
	MaxPooling	0.911-0.975	0.929-0.979	0.959-0.989	0.957-0.989	0.951-0.986
	ABMIL	0.951-0.989	0.947-0.983	0.971-0.994	0.966-0.991	0.953-0.988
	CLAM-SB	0.961-0.993	0.956-0.989	0.980-0.998	0.977-0.995	0.977-0.997
	CLAM-MB	0.963-0.992	0.959-0.990	0.981-0.998	0.980-0.996	0.970-0.994
	DSMIL	0.954-0.992	0.944-0.985	0.954-0.987	0.947-0.984	0.954-0.991
	TransMIL	0.968-0.993	0.959-0.987	0.974-0.995	0.983-0.997	0.981-0.997
	AdditiveMIL	0.961-0.993	0.956-0.989	0.979-0.997	0.978-0.995	0.975-0.996
	SCL-WC	0.952-0.992	0.959-0.990	0.979-0.998	0.981-0.996	0.971-0.994
	LadderMIL (Ours)	0.975-0.996	0.980-0.998	0.989-0.999	0.988-0.998	0.989-0.999
CAMEYLON16	MeanPooling	0.599-0.791	0.559-0.757	0.383-0.588	0.553-0.752	0.503-0.707
	MaxPooling	0.531-0.733	0.569-0.766	0.633-0.819	0.604-0.796	0.553-0.752
	ABMIL	0.484-0.689	0.629-0.816	0.414-0.620	0.626-0.814	0.454-0.661
	CLAM-SB	0.714-0.881	0.661-0.801	0.609-0.800	0.677-0.854	0.719-0.885
	CLAM-MB	0.672-0.850	0.738-0.898	0.582-0.777	0.630-0.817	0.553-0.752
	DSMIL	0.603-0.795	0.553-0.752	0.585-0.780	0.401-0.607	0.533-0.735
	TransMIL	0.589-0.783	0.397-0.604	0.434-0.641	0.577-0.773	0.634-820
	AdditiveMIL	0.717-0.883	0.637-0.822	0.658-0.839	0.702-0.872	0.530-0.731
	SCL-WC	0.693-0.866	0.582-0.777	0.635-0.821	0.578-0.774	0.592-0.786
	LadderMIL (Ours)	0.852-0.969	0.841-0.963	0.738-0.898	0.734-0.896	0.815-0.948

G.4 Fixed thresholds versus Adaptive Threshold Scheduling

Table 16: **Comparison of fixed threshold selection with Adaptive Threshold Scheduling.**

Model	Threshold	Internal (ER)		Internal (PR)	
		AUC	F1-score	AUC	F1-score
LadderMIL (Ours)	Top-5%	0.9118	0.7822	0.8458	0.7564
	Top-10%	0.9130	0.7802	0.8434	0.7400
	Top-15%	0.9154	0.7408	0.8424	0.7476
	ATS	0.9178	0.7848	0.8472	0.7590

G.5 Training Efficiency

Table 17: **Training time compared on the ER classification training set.** The time per epoch is measured as the total time for processing 239 training cases. The comparison is performed with an NVIDIA RTX3060 GPU.

Models	Params	Training Time (s)		Gap vs. LadderMIL
		Per epoch	Avg. per slide	
MeanPooling	2.05K	1.97	0.0067	-0.74
MaxPooling	2.05K	1.9	0.0065	-0.81
ABMIL	0.26M	2.07	0.0071	-0.64
CLAM-SB	0.79M	2.31	0.0079	-0.40
CLAM-MB	0.79M	2.35	0.0080	-0.36
DSMIL	0.15M	2.73	0.0093	0.02
AdditiveMIL	0.79M	2.1	0.0072	-0.61
SCL-WC	0.92M	2.27	0.0077	-0.44
TransMIL	2.67M	3.88	0.0132	1.17
LadderMIL (Ours)	3.28M	2.71	0.0092	0.00

H Interpretability

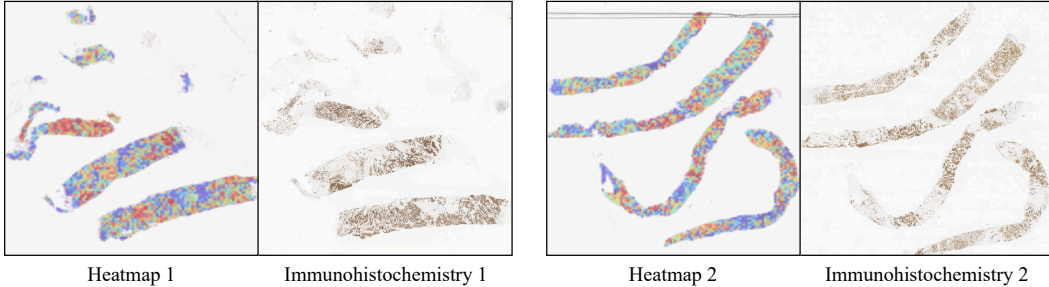


Figure 6: **Heatmap visualisation of LadderMIL.** The heatmaps from two ER+ cases are shown as examples, and compare with their pathological gold standard - immunohistochemistry (IHC) staining. In heatmaps, red denotes high attention while blue denotes low attention. In IHC stained images, brown colour reveals the cells that are considered as ER+.

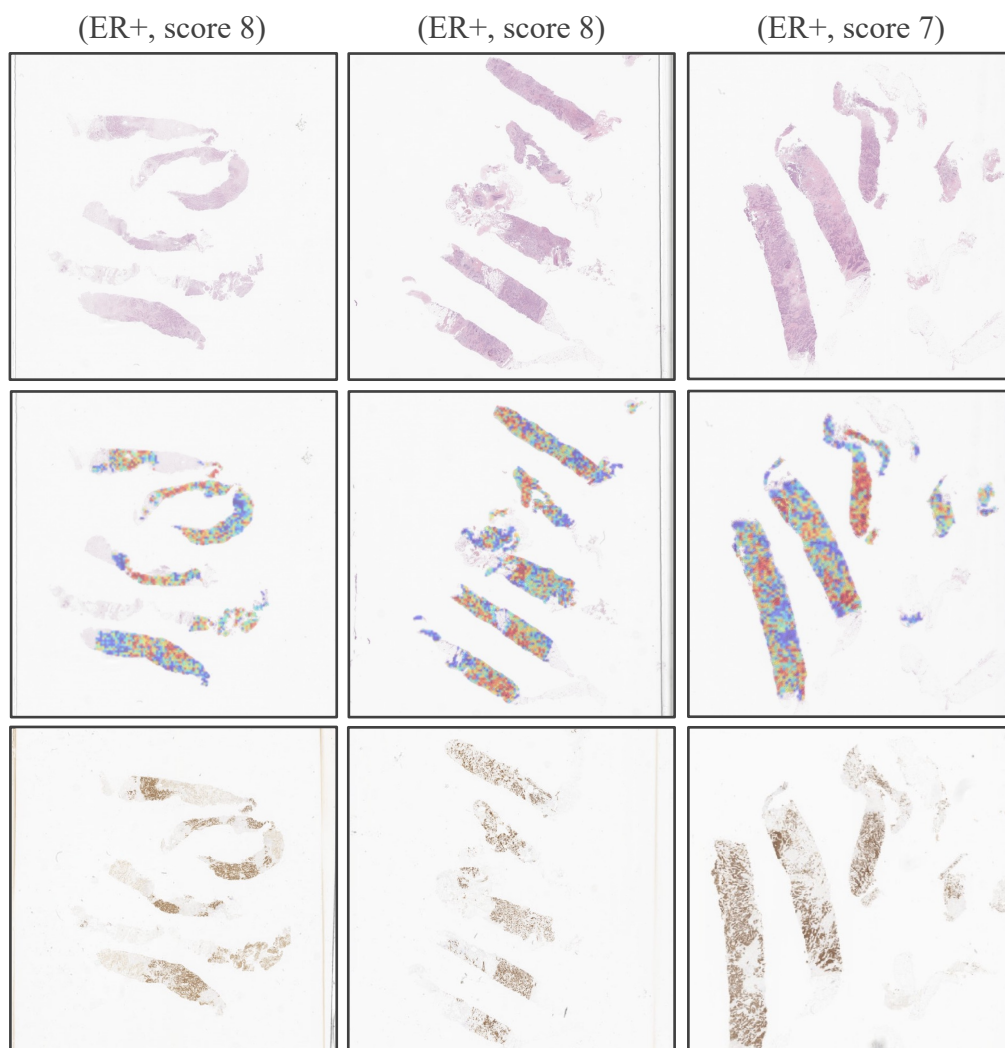


Figure 7: Extra examples for heatmap visualisation of LadderMIL.

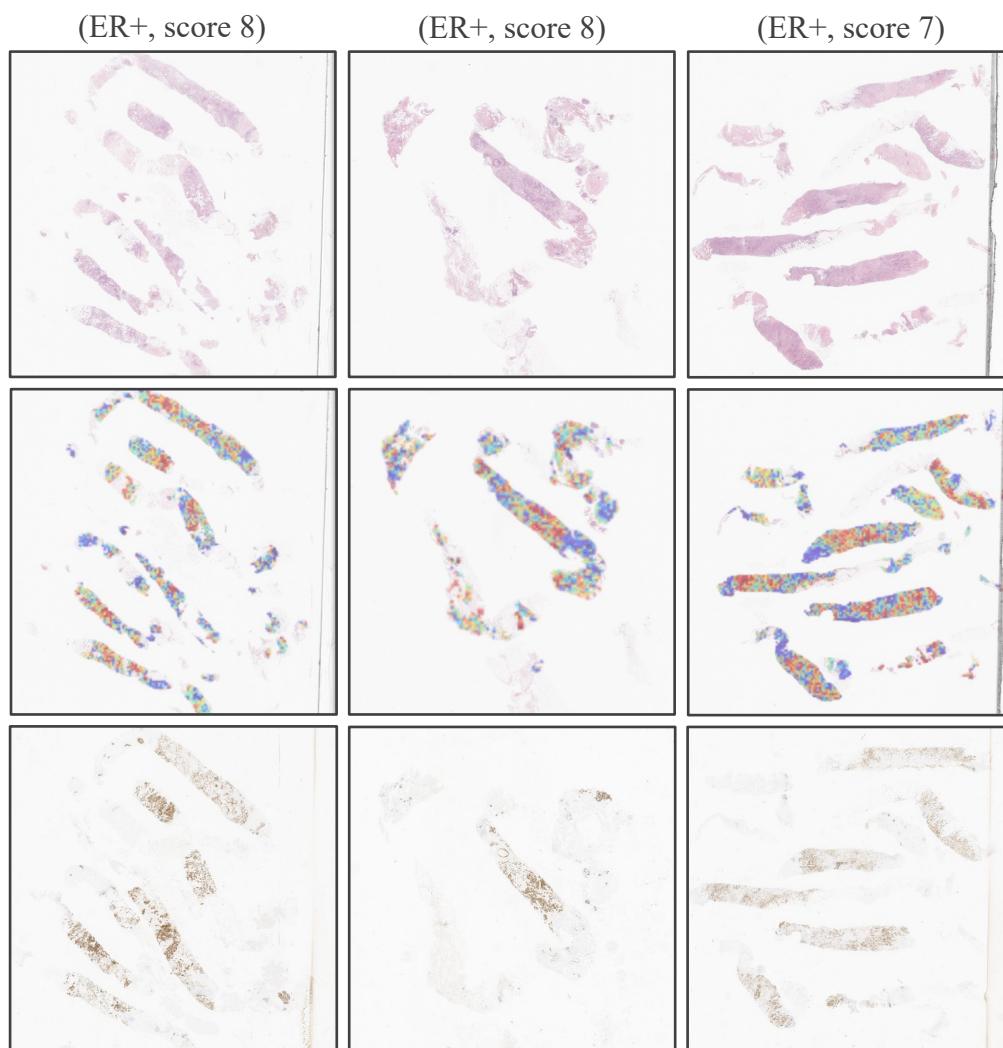


Figure 7: **Continued: Extra examples for heatmap visualisation of LadderMIL.**

I Assets and Licenses

Datasets. We provide the license and URL for the datasets used in this paper.

- TCGA: CC0 1.0 license, since we are using open-access data. The results shown in this paper are in part based upon data generated by the TCGA Research Network: <https://www.cancer.gov/tcga>.
- CAMELYON16 [53]: CC0 1.0 license. The dataset is obtained from the CAMELYON16 Grand Challenge: <https://camelyon16.grand-challenge.org/Home/>.
- Internal Breast Cancer Dataset: Provision and use of whole slide images and associated data for the internal cohort was covered by the approval of anonymity with REF: 20/ES/0061.

Models. We provide the license and URL for the models used in this paper.

- ResNet-50 [42]: MIT license. <https://github.com/KaimingHe/deep-residual-networks>.
- GigaPath [31]: Apache 2.0. <https://github.com/prov-gigapath/prov-gigapath>.
- ABMIL [8]: MIT license. <https://github.com/AMLab-Amsterdam/AttentionDeepMIL>.
- CLAM [9]: GPL-3.0 license. <https://github.com/mahmoodlab/CLAM>
- SCL-WC [11]: GPL-3.0 license. <https://github.com/Xiyue-Wang/SCL-WC>.
- TransMIL [14]: GPL-3.0 license. <https://github.com/szc19990412/TransMIL>
- DSMIL [10]: MIT license. <https://github.com/binli123/dsmil-wsi>.